Dry Metal Forming Open Access Journal

Final Project Report

Edited by Frank Vollertsen
Available online at https://elib.suub.uni-bremen.de

www.drymetalforming.de

Dry Met. Forming OAJ FPR 6 (2020) 334–353
Date of Report 31 May 2020; published 12 June 2020

Polished diamond coatings for dry tapering of aluminum

(DFG Grant No. VO 530/119 Funding Period 01.01.2018 – 31.03.2020)

Markus Prieske*[1], Frank Vollertsen[1,2]

[1]BIAS – Bremer Institut für angewandte Strahltechnik GmbH, Klagenfurter Str. 5, 28359 Bremen, Germany
[2]University Bremen, Bibliothekstr. 1, 28359 Bremen, Germany

Summary

For economic and environmental reasons, dry forming is of increasing interest due to the shortening of process chains, cost savings and reduction of environmental pollution. The aim of these investigations is to examine to what extent CVD diamond coatings are suitable for dry forming of aluminum and to identify the surface topology requirements for a low friction coefficient and low wear. It was discovered that the inner contour of a 5 mm high forming die including undercuts could be coated with a CVD diamond coating of a homogeneous layer thickness by turning the forming die upside down after half the coating time, so that the plasma flame enters through the other opening of the die. Based on oscillating ball on plate tribometer tests and tapering tests it could be shown that for the realization of dry piece goods processes with aluminum material, diamond coatings offer a great potential. It was possible to determine a roughness parameter which is equally capable of predicting the coefficient of friction and the wear rate of the aluminum counter body in the dry oscillating ball on plate tribometer tests for unpolished and mechanically polished CVD diamond coatings. This parameter is the peak material volume (Vmp) and is a measure of the volume of the top 10% of the surface. For dry piece goods processes of aluminum workpieces, the deposition of microcrystalline CVD diamond layers with subsequent post-treatment of the surface is recommended in order to achieve a peak material volume of less than 0.04 ml/m² in order to minimize wear of the aluminum counter body. The lower the Vmp value, the lower the coefficient of friction for the dry contact of diamond with aluminum. Nanocrystalline CVD diamond coatings offer a potential for dry forming of aluminum without post-treatment, but they are more suitable for processes such as wire drawing as they do not withstand repeated static friction. For post-treatment of CVD diamond coatings laser polishing with a picosecond-laser was investigated. It could be shown that the surface roughness could be significantly reduced by 72.5%. As soon as the CVD diamond coating is accessible by laser irradiation, the laser polishing process has a lower risk of delamination of the CVD diamond layer due to lower mechanical stress than applied by mechanical polishing.

Keywords: CVD diamond, polishing, picosecond laser, tapering

1 Motivation

Dry forming is of increased interest for both economic and environmental reasons [1]. Different approaches already lead to a possibility of dry forming. However, tool wear leads to a short tool life, so that dry forming is not yet competitive with lubricated forming processes. Due to their high hardness, wear resistance and chemical inertness against aluminum [2], CVD diamond coatings have excellent preconditions as tool coatings for dry forming. In order to use diamond in forming technology, the deposition of a diamond coating is indispensable for economic and production reasons, as soon as the forming die exceeds the dimension of an inner

*E-mail address of corresponding author: info-mbs@bias.de

diameter of 2 mm [3]. Up to an inner diameter of 2 mm the forming die can be produced out of a single diamond crystal [3].

Tribological investigations show low coefficients of friction for CVD diamond coatings against different materials. Bhushan et al. [4] show a decreasing coefficient of friction with decreasing roughness in the oscillating ball on plate test of aluminum balls against differently smooth polished CVD diamond coatings. This thesis that both the wear rate and the coefficient of friction decrease with a decreasing surface roughness is supported by several publications. Erdemir et al. [5] conclude on the basis of tribometer tests of polycrystalline diamond layers with different roughnesses that the higher the surface roughness, the higher is the friction and the wear rate. The high coefficient of friction of rough polycrystalline CVD diamond coatings is attributed to abrasive ploughing and cutting effects of the sharp surface tips. A higher coefficient of friction in the running-in behavior with a subsequent reduction in the coefficient of friction is explained by the breaking-out and flattening of peaks. Erdemir [6] concludes on the basis of further publications that the general rule is that the smoother the diamond surface, the lower the coefficient of friction and the wear rate. Bögli et al. [7] compare differently treated CVD diamond coatings (mechanically polished, laser polished, plasma polished) with nanocrystalline CVD diamond coatings in a tribometer test. Although the roughness of the surfaces is comparable, the mechanically polished diamond layers (Ra 35 nm) lead to the lowest coefficient of friction of 0.03 against monocrystalline ruby. In contrast the nanocrystalline CVD diamond coatings with a roughness of Ra 30 nm lead to the highest coefficient of friction of 0.57. This clearly shows that the roughness (Ra or Rq) is not a suitable parameter to establish a clear correlation with the coefficient of friction and the wear rate for CVD diamond coatings.

The aim of the project is to enable dry tapering of aluminum rods with CVD diamond coated and laser polished forming dies. Therefore, the CVD diamond deposition on tungsten carbide forming tools as well as laser polishing of CVD diamond coatings by a picosecond laser needs to be investigated. To enable a post processing of the CVD diamond coated forming dies, the entire inner wall of a 5 mm high forming die needs to be coated with a homogenous thickness, which is investigated using an atmospheric laser-based plasma CVD process. For laser polishing of diamond usually nanosecond-laser (graphite formation [8]) or femtosecond-laser (no graphite formation [8]) are used. In this project polishing of CVD diamond coatings using a picosecond-laser is investigated to combine a high removal rate with an interaction time in the range of the free time between lattice collisions to prohibit heating up of the sample and thereby prohibit the formation of graphite.

The scientific objective of this project is to find out whether a surface post-treatment of CVD diamond coatings is necessary for low-wear and low-friction in dry tribological contact with aluminum or whether a targeted adjustment of the process parameters and the associated crystal size and surface roughness is sufficient. The following working hypothesis will be clarified: For mechanically polished and not post-processed polycrystalline diamond surfaces, a decrease in the wear rate of the aluminum counter body and the coefficient of friction can be predicted with the help of a topology size which takes into account the surface properties responsible for the mechanical clamping and the abrasive wear as a result of a decrease in the topology size.

2 Methods and materials

A laser-based plasma (LaPlas) CVD process was used at atmospheric pressure without a vacuum chamber to deposit polycrystalline CVD diamond coatings [9]. The schematic layout of the LaPlas CVD process is shown in Fig. 1. A 6 kW high power CO_2 laser (Trumpf TLF 6000) with the wavelength of 10.6 µm is utilised as an energy supply of an argon plasma jet. The ignition of the plasma flame is achieved by inserting a tungsten lanthanum electrode into the laser focus. After the ignition of the argon plasma flame (26 standard litres per min (slm) Argon), the process gases methane and hydrogen, which are required for CVD synthesis of polycrystalline diamond, are introduced. The summed gas flow of methane and hydrogen was set to 2.0 slm. The methane concentration can be varied from 0.15% up to 5.0% regarding the total gas flow of hydrogen and methane.

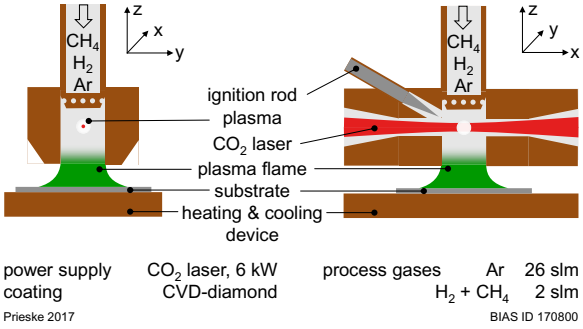

Fig. 1: Schematic layout of the LaPlas CVD process at atmospheric pressure.

Three pyrometers were used for temperature monitoring: IMPAC pyrometer IGAR 12 LO, IP 140 and IGA 10. The K10 hard metal substrate was heated up exemplarily to 800 °C, which was measured by a thermocouple, to determine the emission coefficient for each pyrometer. The emission coefficients were set to 0.98 for the pyrometer IGAR 12 LO and IP 140 and to 0.86 for pyrometer IGA 10. A feedback control was implemented, which regulates the laser power according to the substrate temperature measured by the IMPAC pyrometer IGAR 12 LO to ensure a constant deposition temperature over the deposition time of 20 minutes. Detailed information about the implementation of the feedback control is published in [10]. The measuring accuracy was ±10 K due to the remaining inaccuracies of the determined emission coefficients and the feedback control.

As substrate material metal discs with a diameter of 20.3 mm and a thickness of 3.00 mm ± 0.15 mm were used. The flat substrate and forming dies are both manufactured out of K10 hard metal of the type CTF12D consisting out of 94% tungsten carbide and 6% cobalt. The geometry of the forming die can be seen in Fig. 2. The substrates and the dies were etched by Murakami reagent ($K_3Fe(CN)_6$: KOH : H_2O = 1:1:10) for 30 minutes and subsequently with Caro's reagent (3 ml 96 wt% H_2SO_4, 88 ml 40% w/v H_2O_2) [11]. The diamond nucleation was carried out with a dispersion consisting of 200 ml of isopropanol and 210 mg of diamond powder with an average crystal size of 0.25 µm to 0.50 µm from the company Microdiamant AG. The substrates were put into the dispersion for ten minutes in an ultrasonic bath and subsequently into isopropanol for three minutes. Regarding the forming dies the areas that should not be nucleated were masked before nucleation.

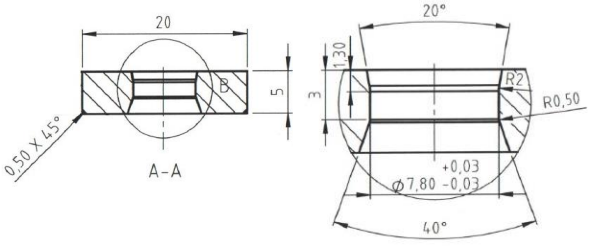

Fig. 2: Technical drawing of the hard metal forming die.

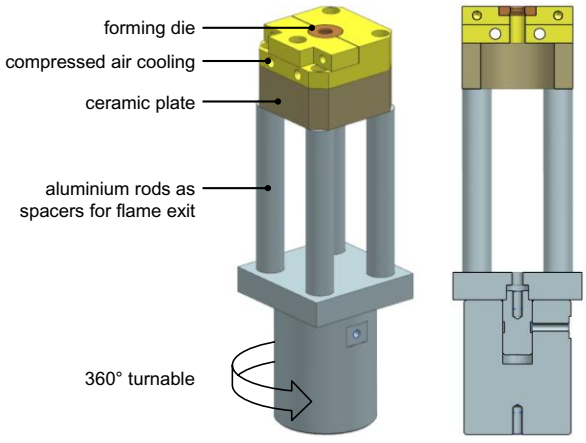

Fig. 3: Substrate holder for the diamond deposition of a forming die.

The specially produced substrate holder for the forming dies is shown in Fig. 3. The substrate holder consists of a two-piece brass part to clamp the forming die onto the table. In addition, there are two holes for compressed air cooling and a hole below the die opening which allows the plasma flame to exit at the other end. The ceramic plate underneath serves as thermal insulation. In order to increase the homogeneity in radial direction, the table is freely rotatable during the coating process.

A picosecond-laser TruMicro 5050 of the company Trumpf with a wavelength of 515 nm, a maximum pulse energy of 150 µJ and a maximum repetition rate of 200 kHz was used. The laser ablation was performed under an inclination angle of 80°. This is done to transfer the polishing process more easily to the tapering zone of a forming die as well as due to the fact, that Tokarev et al. [12] achieved the lowest roughness by laser polishing with an angle of incidence between 75° and 80°. For the investigations of laser ablation microcrystalline CVD

diamond coatings were deposited at a deposition temperature of 1050 °C and a hydrogen methane ratio of 2% with a thickness of 12 µm.

Scanning electron microscopy (SEM) (Carl Zeiss Microscopy EVO MA-10), digital microscopy (Keyence VHX-1000) and 3D laser scanning confocal microscopy (Keyence VK 9710) were used to take images of the coating surfaces and measure the coating thicknesses, as well as the average crystal sizes. The surface roughness of the different coatings was measured by the laser scanning confocal microscope according to DIN EN ISO 25178. An energy dispersive X-ray spectroscopy (EDX) (Bruker Nano GmbH XFlash Detector 610M) integrated into the SEM was applied for element analyses and mapping measurements. Micro-Raman spectroscopy (Renishaw system 1000) enabled the detection of diamond and graphite by using the excitation wavelength of 514 nm and a laser power of 25 mW. The spot size of the laser beam was 10 µm in diameter and the spatial resolution of the spectrometer was 1.6 cm^{-1}. The existence of diamond was proofed by the measurement of the first order Raman line of diamond at 1332 cm^{-1} [13]. The G-band at 1560 cm^{-1} [14] in the Raman spectra, was utilized to detect graphite in the deposited coatings. Equation (1) [15] was used to calculate the diamond quality factors Q of the deposited coatings using the peak intensity of the diamond Raman line I_D and the intensity of the G-band peak I_G. The diamond quality factor allows for a semi-quantitative estimate of the quality of a diamond coating, i.e., the concentration of the sp^3-bonds compared to sp^2-bonds.

$$Q = I_D \cdot (I_G + I_D)^{-1} \quad (1)$$

Cryofractures were prepared to accurately determine the coating thickness. A slit was eroded in the backside of the sample up to 500 µm below the surface by electrical discharge machining. Afterwards, the specimens were cooled down by liquid nitrogen and cryofractures were carried out.

Dry tribological oscillating ball on plate tests were performed using a CETR Universal Mechanical Tester UMT-3MT. All tests were carried out according to DIN EN 1071-12 standards. A surrounding climate chamber kept the environmental conditions constant at a temperature of 24°C ± 1°C and 40% ± 1% relative humidity. To examine the long-term behavior of different diamond coatings, a total sliding distance of 1 km was chosen, corresponding to 99,900 cycles along a linear sliding length of 10 mm. The velocity was set to 50 mm/s and the contact force was set to 10 N ± 0.2 N leading to a Hertzian contact pressure of 759 MPa [16]. The aluminum alloy EN-AW-5083 (AlMg4.5Mn0.7), which is commonly used in the automotive industry [17], was used as counter body material. On the one end of an aluminum rod, a hemisphere with a radius of 5 mm was lathed, which was used as counter body. Before testing, the surfaces of the coated plates and round-ended aluminum pins were cleaned with ethanol in an ultrasonic bath for a duration of five minutes. After testing, the wear rates for the round-ended pins were calculated, which is described in detail in [18].

Nine different diamond coatings were deposited by varying the methane/hydrogen ratio, the deposition duration and temperature, which are listed in Table I. The different surfaces of the diamond coatings are shown in Fig. 4. For the designation of the different CVD diamond coatings the mean crystal size is used. The CVDD 10.25p coating was mechanically polished by the company ‘Diamond Product Solutions’, which is marked by the letter ‘p’. In case of the coatings CVDD 8.89r and CVDD 1.91r two samples were rubbed against each other which led to a mechanical polishing of the diamond surface, which is marked be the letter ‘r’.

Table I: Process parameters and sample designation of the different deposited CVD diamond coatings.

designation	temperature	time/ min	CH_4/H_2	thickness/ µm	mean crystal size/ µm	Sa/µm	remark
CVDD 10.25p	1050 °C	40	2 %	14.0	10.25 ± 3.20	0.02	polished, TZM substrate
CVDD 9.70	1050 °C	40	2 %	14.6	9.70 ± 3.04	2.09	
CVDD 8.89r	1050 °C	40	2 %	14.6	8.89 ± 3.50	1.47	rubbed
CVDD 4.71	1050 °C	20	2 %	6.0	4.71 ± 0.98	1.24	
CVDD 1.91r	900 °C	20	1 %	3.0	1.91 ± 0.28	0.84	rubbed
CVDD 1.86	900 °C	20	3 %	3.4	1.86 ± 0.58	1.27	
CVDD 1.66	900 °C	12	3 %	2.0	1.66 ± 0.54	0.94	
CVDD 0.94	900 °C	12	1 %	1.8	0.94 ± 0.26	0.85	
CVDD 0.48	750 °C	15	5 %	1.4	0.48 ± 0.11	0.68	nanocrystalline

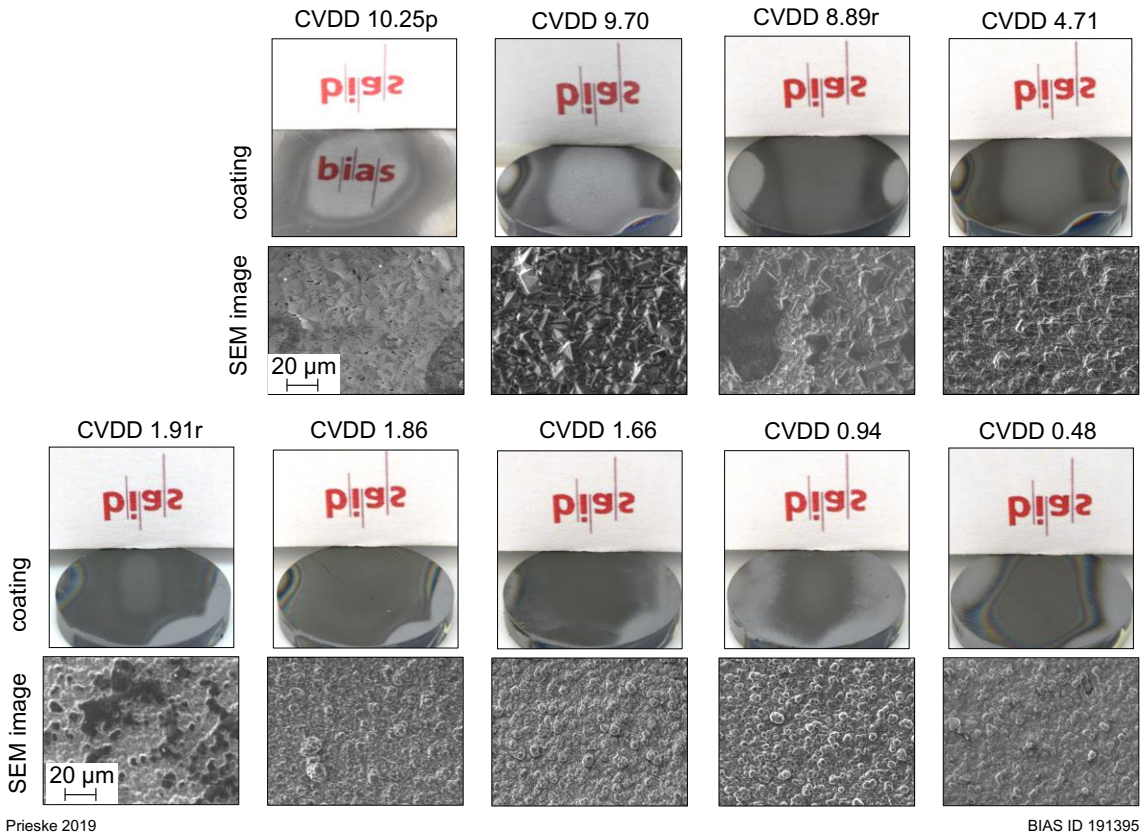

Fig. 4: Different CVD diamond layers used as a plate: a photo with reflection of the bias institute logo on top and a secondary electron (SE) image on the bottom.

A Zwick Roell Z250 testing machine with a maximum press force of 250 kN was used to carry out the tapering processes. The designed device for the tapering process is shown in Fig. 5. The workpiece has a clearance of 0.2 mm in diameter within the guidance, which is typical for tapering processes [19 p. 236]. The forming process can be carried out with the testing machine used at a maximum stamping speed of 10 mm/s. The machine is programmed to move the punch 20 mm downwards. After the taper process, the samples are taken out from the forming tool in the reverse direction with a hydraulic ejector.

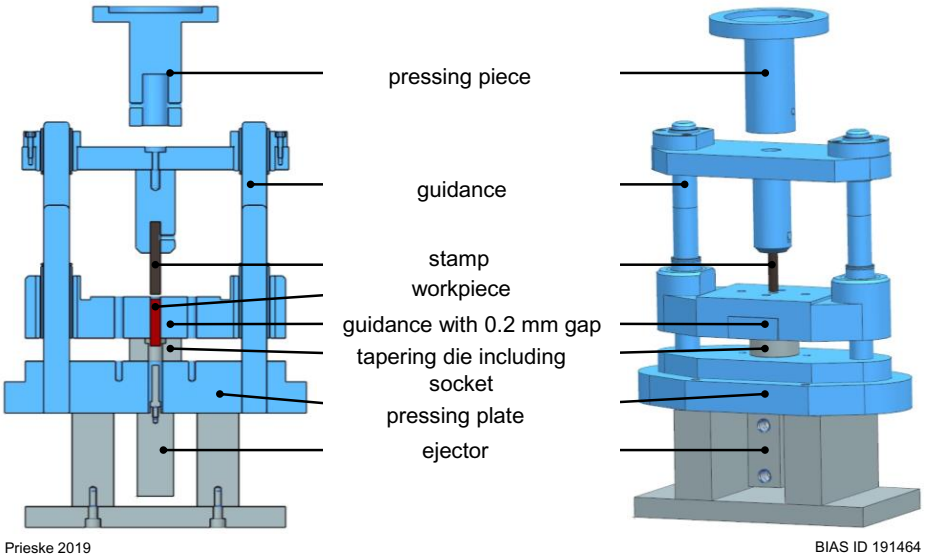

Fig. 5: Construction of the forming test stand for tapering including ejector in the cross-sectional view (left) and in the 3D representation (right).

3 Results

In Fig. 6, the investigated process window for the polycrystalline CVD diamond deposition onto hard metal is shown by illustrating the corresponding crystal sizes by size of the marks. The applied etching process at the

K10 hard metal substrates lead to an etching depth of the cobalt binder of 9 µm. The results show that coatings are deposited in the examined temperature range from 650 °C to 1100 °C. A methane concentration of 0.15% is too low for achieving a deposition in case of all process temperatures carried out. For methane concentrations of 0.25% and 0.5%, depositions were achieved up to 800 °C and 1000 °C, respectively. For methane concentrations from 1.0% to 5.0%, all investigated temperatures result in coating depositions. With increasing process temperature, the crystal sizes firstly increase before they decrease again with further increasing temperature. The same behavior can be seen for an increasing methane concentration.

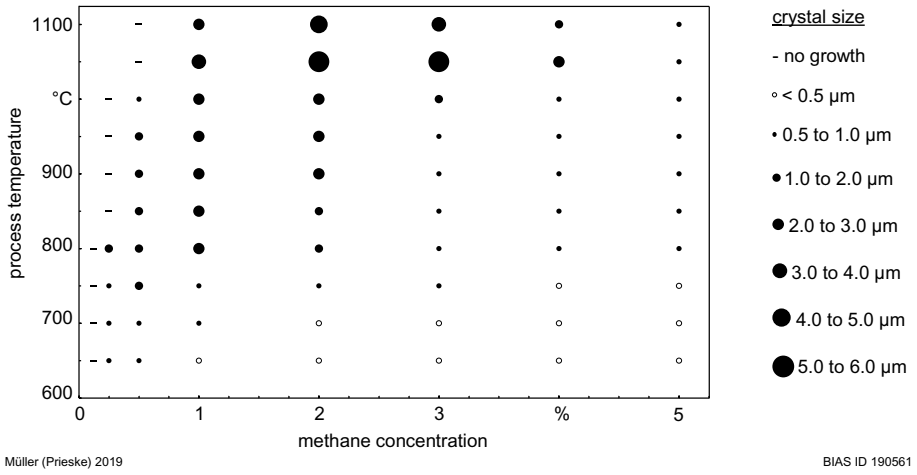

Fig. 6: Process window of the LaPlas CVD process with mean crystal sizes of the corresponding coatings as a function of the process temperature and the methane concentration.

For samples produced with methane concentrations below the process window (stated by "no growth" in Fig. 6) the Raman measurements showed no peak in the recorded spectrum, as can be seen in Fig. 7a for a coating deposited at 1050 °C and a methane concentration of 0.5%. In case of concentrations in the middle of the process window, the coatings show a clear diamond peak in the Raman spectrum, as is shown exemplarily in Fig. 7b for a coating deposited at 1050 °C and the methane concentration of 2.0%. Here a diamond quality factor of 0.85 was reached. The Raman spectrum of the coatings show an increasing G-band graphite peak while only a small diamond peak is formed when the methane concentrations are high and therefore close to the right-hand side of the investigated process window. This is seen in Fig. 7c for a coating deposited at 1050 °C and a methane concentration of 5.0%. The diamond quality factor of this coating is determined to be 0.62.

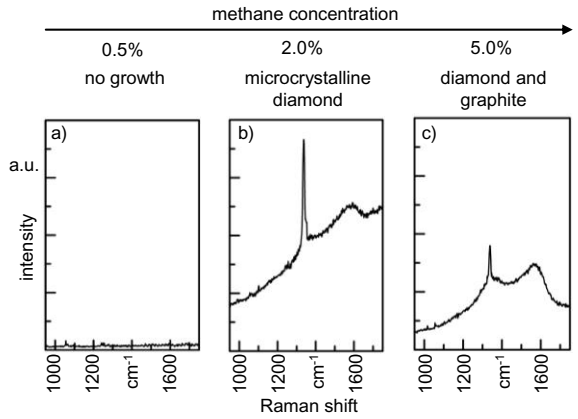

Fig. 7: Raman spectra of coatings deposited at the process temperature of 1050 °C and different methane concentrations: (a) 0.5%; (b) 2.0%, and (c) 5.0%.

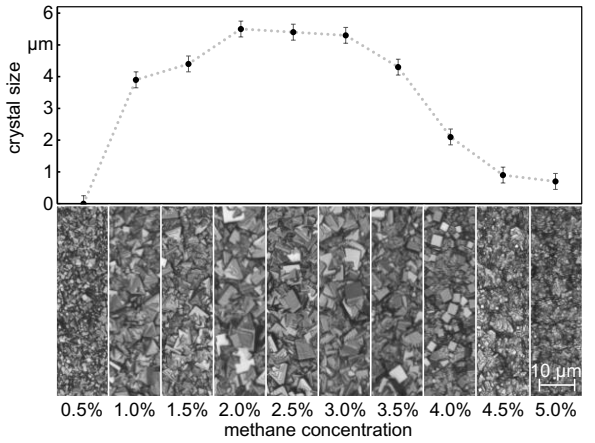

Fig. 8: Crystal size as a function of the methane concentration for the deposition temperature of 1050 °C and the coating time of 20 min.

The average crystal sizes of the coatings deposited at the temperature of 1050 °C were measured. The determined values are given in Fig. 8 as a function of the methane concentration. For the methane concentration of 0.5%, no coating is deposited. The tungsten carbide substrate surface is still visible after the process. For increasing concentrations up to 2.0%, the crystal size also increases up to 5.5 µm. Until the concentration of 3.0% is reached, the crystal size decreases slightly to around 5.3 µm. In the case of higher methane concentrations, the crystal size decreases to less than 1 µm at 5.0% methane.

The coating thickness of the samples, synthesized with the deposition time of 20 min, was measured by using cryofractures. The coating thickness as a function of the methane concentration is given in Fig. 9 for different process temperatures. For increasing methane concentrations and deposition temperatures, the coating thickness increases. However, the coating thickness saturates for increasing methane concentrations at each temperature. In contrast to the visible tendency in the relation between temperature and coating thickness, the process temperature of 1050 °C corresponds to the thickest coating on the hard metal substrates. The coatings deposited at the process temperature of 1100 °C are clearly thinner in comparison to the 1050 °C samples. In the case of the temperature of 1050 °C and the methane concentration of 3.0% (middle of the process window), the coating thickness of 6.5 µm was reached after 20 min of deposition. A microcrystalline diamond coating was deposited (see Fig. 8). The diamond coating deposited at the methane concentration of 5.0% and the deposition temperature of 1050 °C reaches a coating thickness of 6.8 µm even though the crystal size is smaller than one micrometer (see Fig. 8).

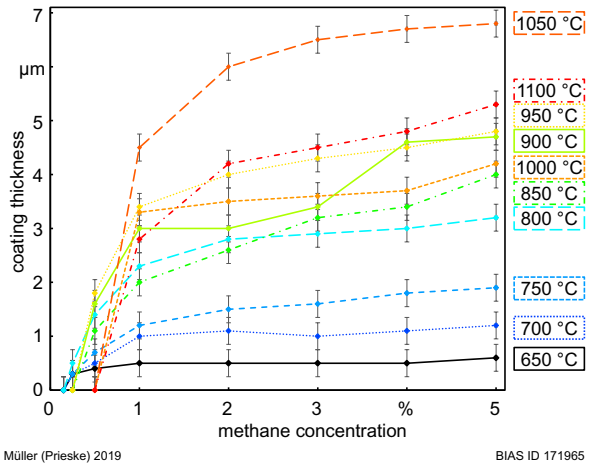

Fig. 9: CVD diamond coating thicknesses after 20 min of deposition for different process temperatures and methane concentrations.

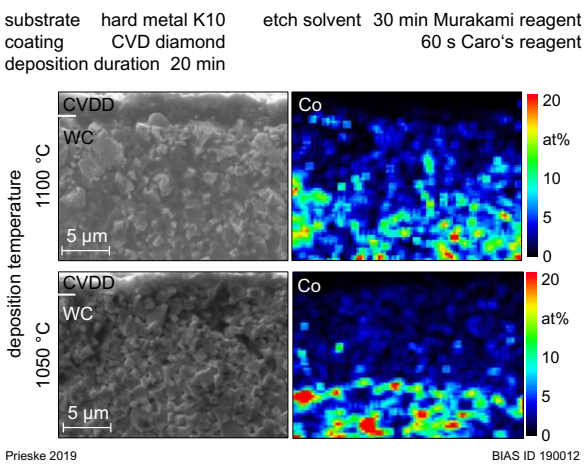

Fig. 10: Secondary electron images (left) and EDX mappings (right), which show the percentage distribution of cobalt in cryofractures after the deposition at the process temperatures of 1100 °C (a) and 1050 °C (b).

In order to check whether the unexpected behavior of the coatings deposited at 1100 °C is due to an onset of cobalt diffusion, an EDX mapping was performed, which is given in Fig. 10. At the process temperature of 1050 °C, the EDX mapping (Fig. 10b) shows a relatively clear limit of the cobalt binder removal by the etching process and that cobalt had not diffused to the surfaces of the substrate after the coating process. This clear boundary is no longer present after a coating process at 1100 °C (Fig. 10a).

Coatings with different deposition times were produced to find out if a coating thickness could be converted directly into a growth rate. In Fig. 11, the coating thickness is depicted as a function of the deposition time. After the deposition time of 2.5 min, a thin coating could be seen. EDX measurements show 96% carbon content on the surface. An optically closed 1.3 µm thick coating was deposited when increasing the deposition time to five minutes. The measured carbon content of the surface for this coating is 98%. A further increase of the deposition time results in a linear increase of the coating thickness. Therefore, the data given in Fig. 11a were used to determine the constant growth rate of 22 µm/h for the given process parameters. The results of the process window of the LaPlas CVD process on hard metal are published in [21].

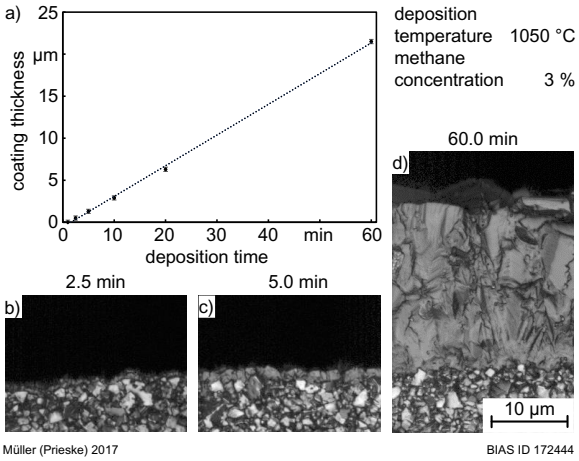

Fig. 11: (a) The trend of the growth rate for different deposition times at the temperature of 1050 °C and the methane concentration of 3% and cryofractures of the coatings after the deposition times of (b) 2.5 min, (c) 5 min and (d) 60 min.

At first the hard metal was etched for 30 minutes by Murakami reagent to roughen the surface. Afterwards Caro's reagent was applied to etch the cobalt binder near the surface. To ensure for the forming dies that the cobalt binder was removed near the surface so that the diamond coating could be deposited without the influence of cobalt, the etching time of Caro's reagent was varied, and the etching depth analyzed. On the one hand, the cobalt binder is to be removed sufficiently deep and at the same time a change in the geometry of the carbide due to the removal of tungsten carbides must be avoided. In Fig. 12 it can be seen, that at the beginning of the etch process, the etching rate is relatively high and decreases afterwards. After 90 seconds tungsten carbides start to be removed out of the surface. As a result of the investigations, the forming dies were etched for 45 seconds.

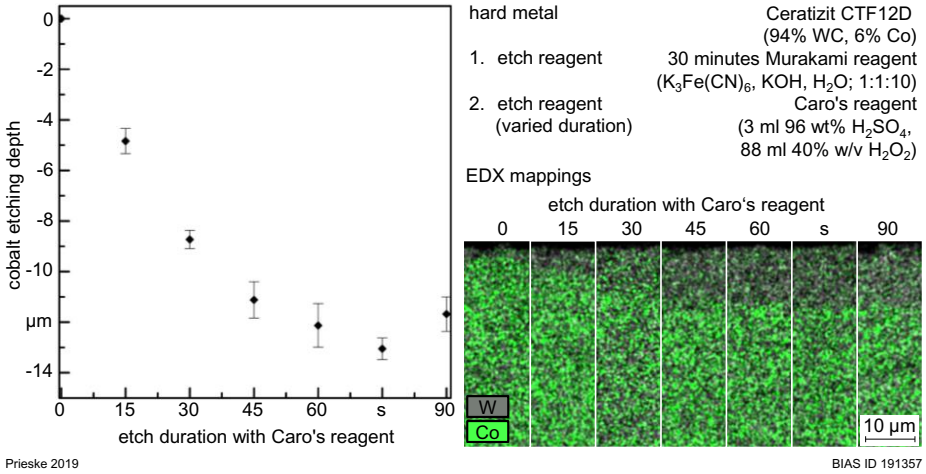

Fig. 12: Cryofractures of etched hard metal substrates with varied etching duration by Caro's reagent with the measured etching depth of cobalt and corresponding EDX mappings

Fig. 13 shows that without masking during nucleation the flat area at the top of the forming die is coated by a closed CVD diamond coating. The CVD diamond coating at the top side partly detaches or totally delaminates after the deposition process and also leads to a crack formation of the CVD diamond coating in the forming zone (compare Fig. 13 right). In the case of masked diamond nucleation, no layer detachment is detected as can be seen in Fig. 14. The closed diamond coating ends at a distance of 28 µm ± 3 µm from the edge of the forming zone.

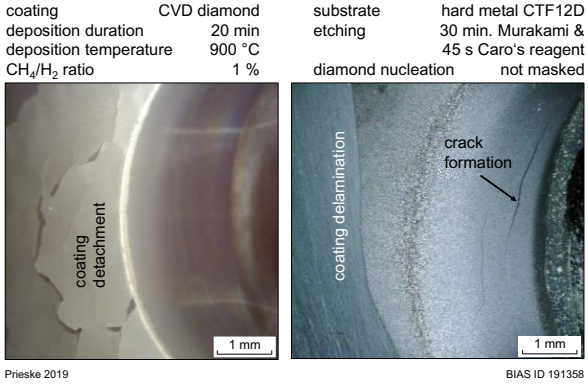

Fig. 13: Microscope images of the CVD diamond coated forming die with usual diamond nucleation.

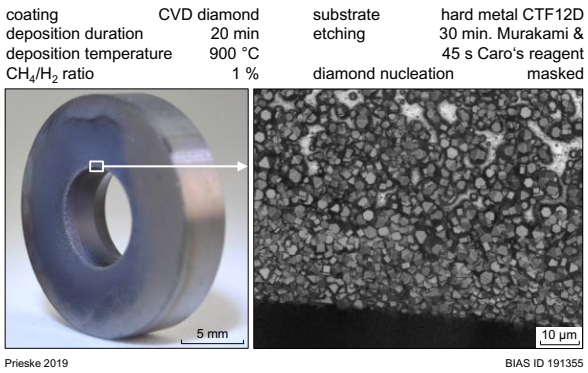

Fig. 14: Photography and microscope image of the CVD diamond coated forming die with masked diamond nucleation.

Fig. 15 shows a cryofracture of a CVD diamond coated forming die. The coating was deposited for twenty minutes through the entrance opening of the forming die. It can be seen that the entire inner wall including undercuts of the forming die is coated. The coating thickness at the entrance opening where the plasma flame enters (Fig. 15 *top* section of forming die) is 1.0 µm ± 0.1 µm. Towards the bottom of the inner wall the coating thickness decreases down to 0.4 µm ± 0.1 µm. That leads to the mean coating thickness of 0.7 µm ± 0.3 µm.

Fig. 16 shows the result when the coating is deposited through both openings. To do this, the CVD diamond deposition through the entrance opening is stopped after twenty minutes and the forming tool is re-clamped upside down in the substrate holder before the restart of the process. The coating is then deposited for an additional twenty minutes by entering through the exit opening. This procedure leads to the mean coating thickness of 2.3 µm ± 0.1 µm.

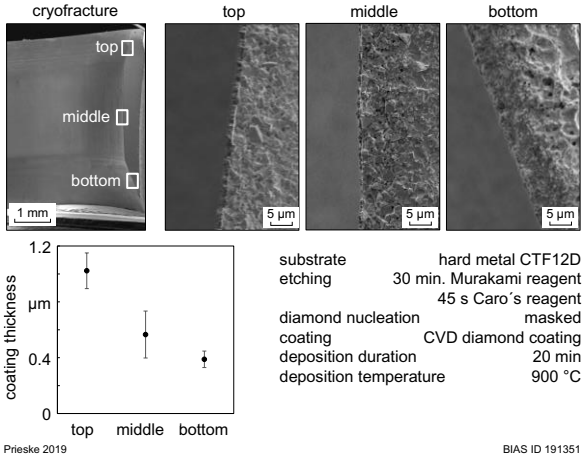

Fig. 15: SEM images of a cryofracture of a CVD diamond coated forming die after deposition through the entrance opening as overview (left) and as detailed images and the coating thickness in axial direction (bottom left).

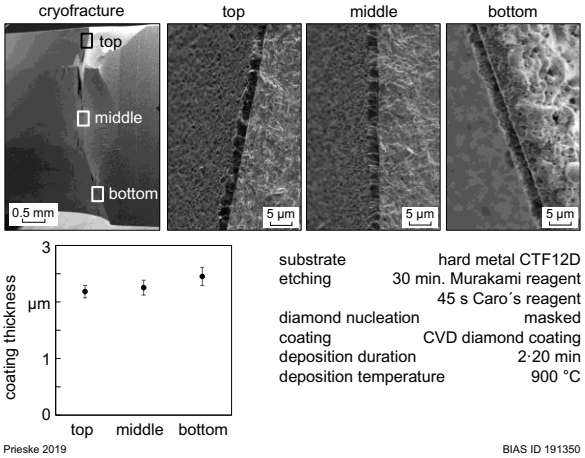

Fig. 16: SEM images of a cryofracture of a CVD diamond coated forming die after deposition through the entrance and the exit opening as overview (left) and as detailed images and the coating thickness in axial direction (bottom left).

The distribution of the diamond crystal size along the inner wall varies depending on whether a one-sided or two-sided deposition was applied, as can be seen in Fig. 17. The procedure of the one-sided deposition shows a decreasing crystal size towards the bottom of the forming die. In case of the two-sided deposition, the crystal size at the top and bottom of the die is approximately the same. At the middle position, the diamond crystal size is 0.4 µm smaller than at the top and bottom. The results of the CVD diamond coating of forming dies are published in [22].

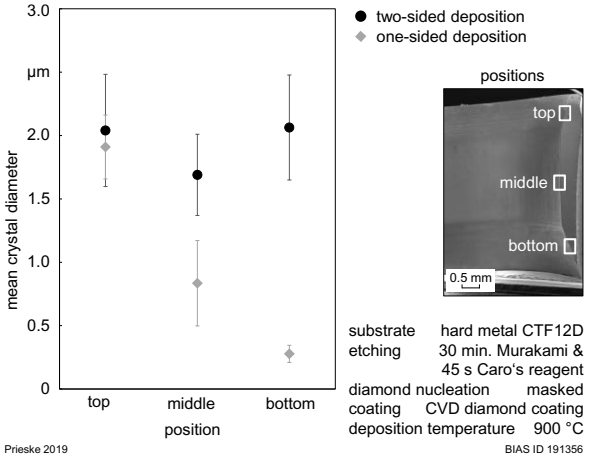

Fig. 17: Comparison of the mean diamond crystal diameter at different positions of the inner wall after one- and two-sided deposition.

After deposition the surface needs to be polished, in this case by laser ablation. The determination of the threshold fluence is shown in Fig. 18. The confocal laser-scanning images show a clear ablation with a fluence of 0.36 J/cm² and higher, so that the threshold fluence is determined at 0.36 J/cm² with a pulse energy of 10.5 µJ.

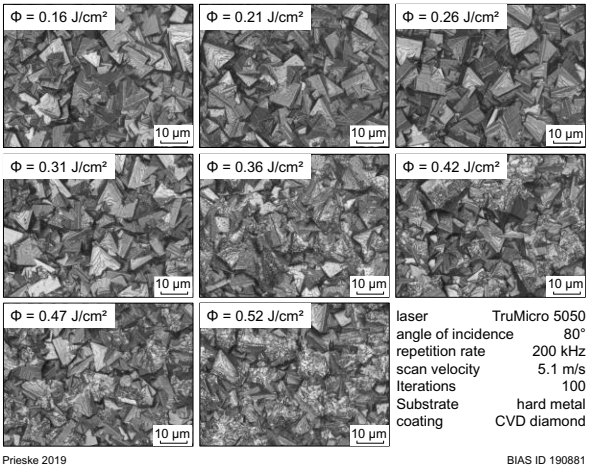

Fig. 18: Confocal laser-scanning images of the CVD diamond surface after ablation with different laser fluences.

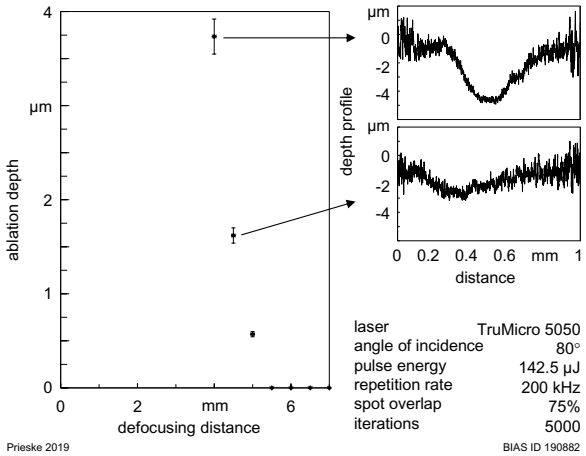

Fig. 19: Ablation depth depending on laser defocusing distance.

The low threshold fluence of 0.36 J/cm² at a pulse energy of 10.5 µJ enables the processing of a larger area by defocusing the laser with a simultaneous increase of the pulse energy up to the maximum pulse energy of 150 µJ. Fig. 19 shows the ablation depth after 5000 iterations using a fixed pulse energy of 142.5 µJ at different defocusing distances. A defocusing distance of 5.5 mm and higher leads to no ablation of the CVD diamond coating. The ablation depth of 3.7 µm as a result of a defocusing distance of 4.0 mm leads to a trench, which can be seen in the height profile. The formation of a trench makes the polishing of a large area difficult and should be avoided. Therefore, the following studies were performed with a defocusing distance of 4.5 mm, which leads under an inclination angle of 80° to the polishing of a track width of 600 µm.

Fig. 20 shows the initial arithmetic mean height Sa compared to the Sa after different numbers of polishing processes. After each area polishing process, the sample is rotated by 90°. After four polishing processes the arithmetic mean height can be reduced by 72.5% from 1.85 µm ± 0.13 µm to 0.51 µm ± 0.01 µm. Micro-Raman spectra of the unpolished and polished CVD diamond surfaces are shown in Fig. 21. The first order Raman line, which is shifted to 1339 cm^{-1} can be detected on all surfaces [20]. That means due to a shift of the Raman line by 7 cm^{-1}, that the coatings have a residual compressive stress of 2.4 GPa [23]. To compare the graphite content of the CVD diamond surfaces the ratio between the intensities of the diamond first order Raman line I(diamond) and the G-band I(G) at 1580 cm^{-1} was calculated [24]. The ratio I(diamond)/I(G) for all diamond coatings was 1.3. The resulting surfaces of the CVD diamond coatings are shown in scanning electron microscope images in Fig. 22. The results of laser polishing of CVD diamond by a picosecond laser are shown in [25].

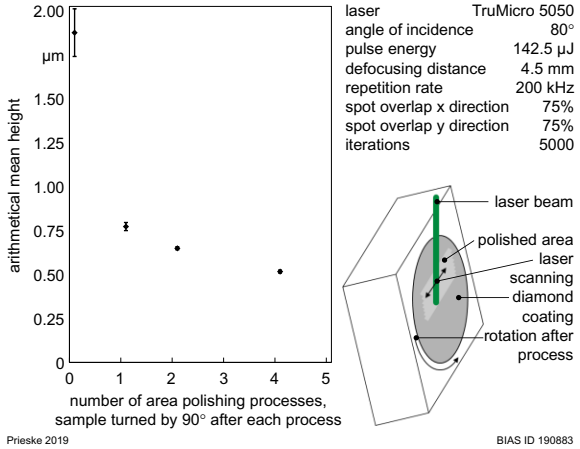

Fig. 20: Resulting arithmetical mean height depending on number of area polishing processes.

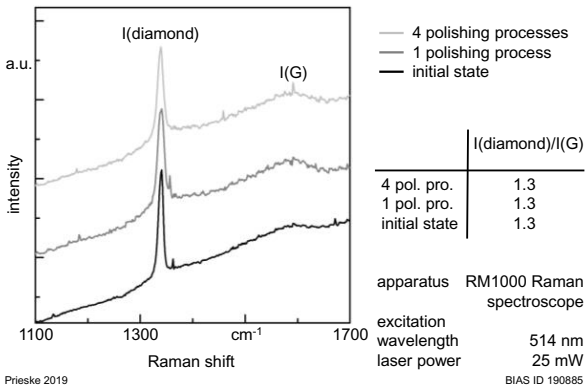

Fig. 21: Micro-Raman spectra of initial state and after one and four polishing processes.

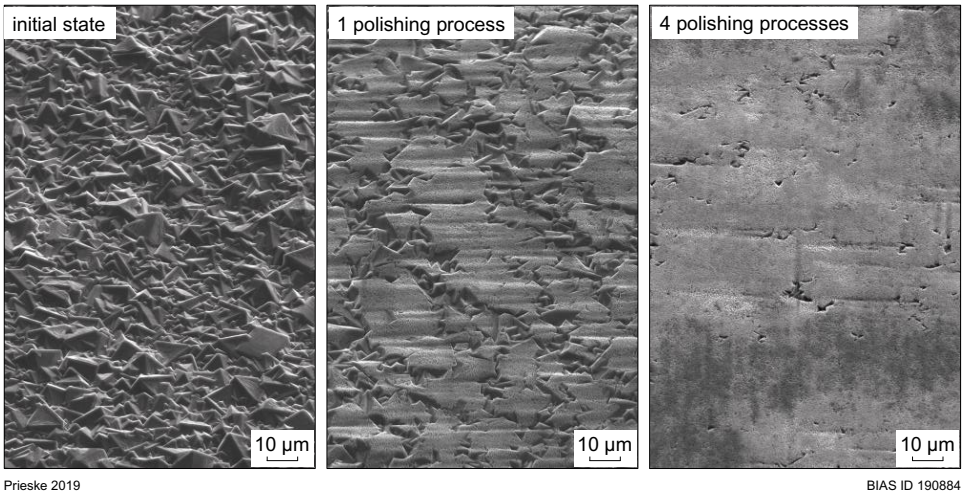

Fig. 22: Scanning electron microscope images of the CVD diamond surfaces.

The mean values of the friction coefficients over the first, middle and last half hour of the 5.5 hour oscillating ball on plate tribometer test of different CVD diamond coatings against aluminum balls are shown in Fig. 23. Of all coatings, the CVDD 10.25p coating shows the most constant behavior over the entire test period. The coefficients of friction of the CVD diamond coatings clearly show the influence of the coating surface in dry tribological contact with aluminum. At the beginning of the tribometer test, the coefficient of friction is between 0.13 and 0.58 depending on the coating surface. In the last half hour of the test, the coefficients of friction of the CVD diamond coatings are between 0.12 and 0.48. The wear rates of the aluminum balls after the tribometer tests are shown in Fig. 24. It can be seen that the three diamond coatings with the largest crystal size, which were not post-treated, lead to the largest wear rates of the aluminum balls. The polished diamond coating CVDD 10.25p leads to the smallest wear rate of the aluminum ball of $4.5 \cdot 10^{-9}$ mm³/Nm.

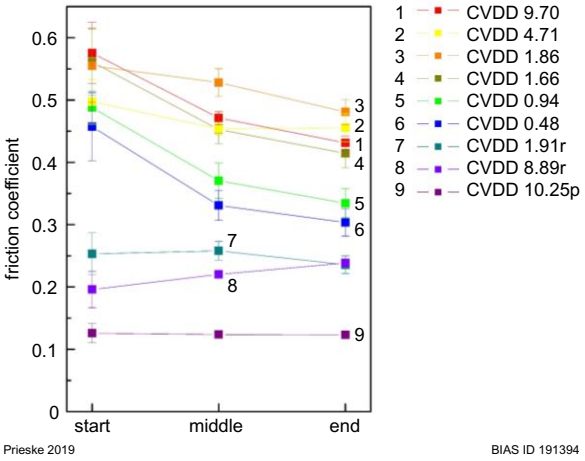

Fig. 23: Average friction coefficient over 9,000 cycles at the beginning, middle and end of tribological examination.

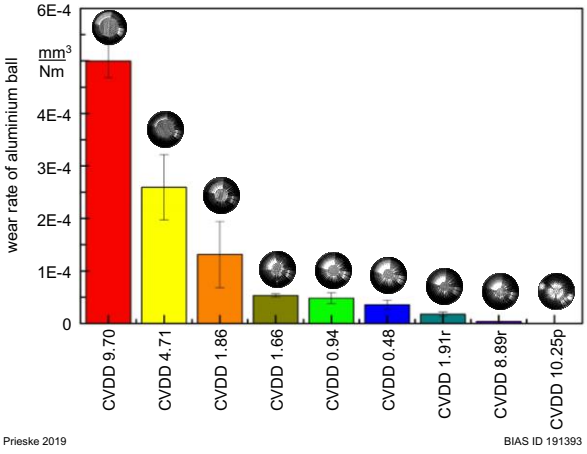

Fig. 24: Wear rate of the aluminum ball after the tribometer test against the different diamond layers as well as an image of the ball after the test.

The two coatings with the smallest mean crystal size CVDD 0.48 and CVDD 0.94 show coating delamination at the turning points of the oscillating ball on plate test. In Fig. 25 the delamination is exemplarily shown for CVDD 0.94. This can only be detected at the turning points, in the remaining wear track neither layer detachments nor crack formations of the diamond coating are detected. The calculated diamond quality factors before and after the tribometer test are shown in Fig. 26. The fact that in each case the diamond quality factor could be determined before and after the tribometer test shows, that in no case the diamond coating is worn out in the center of the wear track. The tribometer test does not lead to a change of the diamond quality factor. Furthermore, it can be seen, that the diamond quality factor increases with increasing mean crystal size.

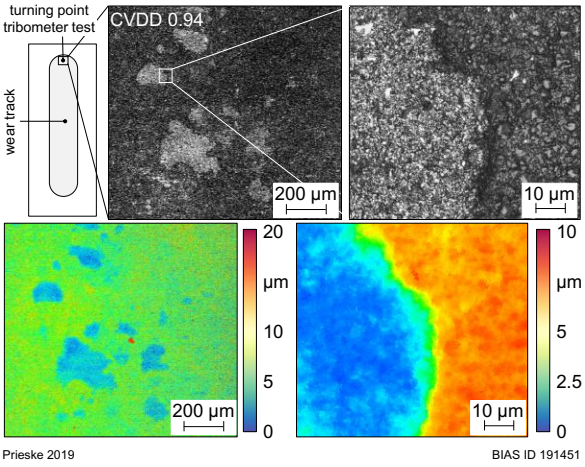

Fig. 25: Coating delamination at the turning point of the CVDD 0.94 coating as confocal microscope image and height image.

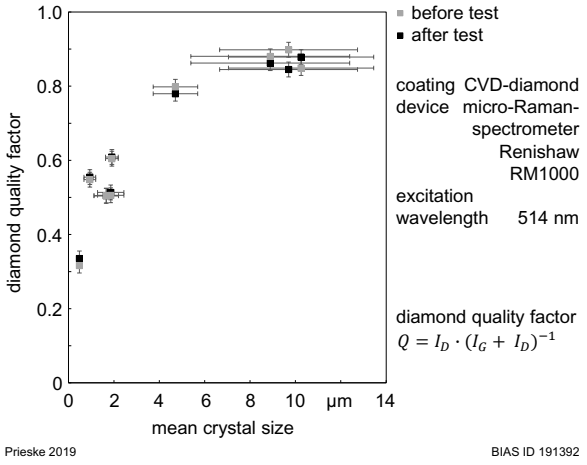

Fig. 26: Diamond quality factor of the CVD diamond coatings depending on the mean crystal size before and after the tribometer test.

Fig. 27 shows the coefficients of friction determined in the tribometer test as a function of various parameters for describing the surface roughness (core material volume (Vmc), reduced valley depth (Svk), peak extreme height (Sxp) reduced peak height (Spk)). It is noticeable that in all four diagrams, two mechanically polished samples differ from the other samples. These are the two samples which were mechanically polished by rubbing two diamond layers against each other.

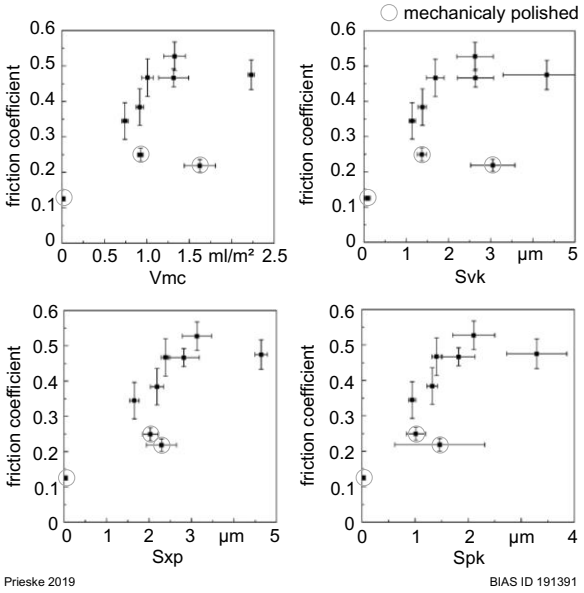

Fig. 27: Mean coefficient of friction as a function of different parameters of surface roughness.

The mean coefficient of friction as a function of the arithmetical mean height Sa as well as of the peak material volume Vmp is shown in Fig. 28. A comparable relationship can be recognized. However, it is noticeable that two mechanically polished coatings are not in line with the relationship in the diagram of the arithmetical mean height. The friction coefficient increases with an increasing Vmp and saturates over a Vmp value of 0.1 ml/m².

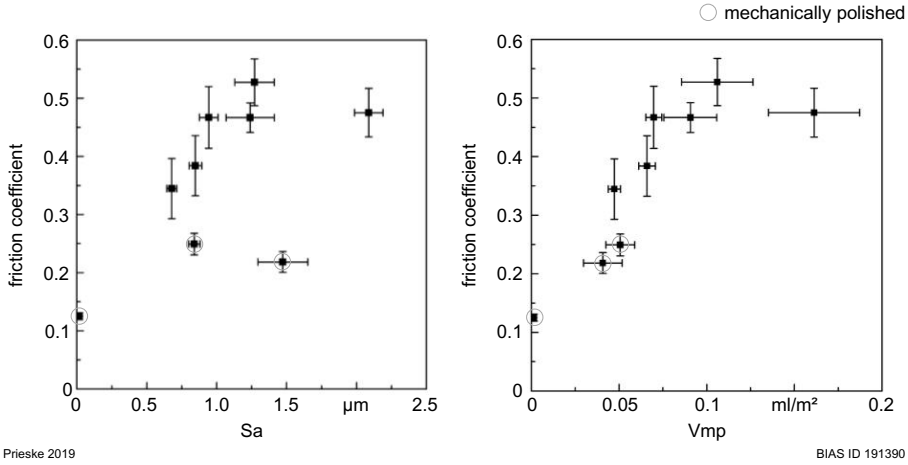

Fig. 28: Mean coefficient of friction as a function of the arithmetical mean height as well as of the peak material volume.

The same behavior, that two mechanically polished diamond coatings do not show the relationship of the unpolished coatings, can be seen regarding the wear rate of the aluminum ball as function of the Sa in Fig. 29 (left). In contrast, the wear rate of the aluminum ball as a function of the Vmp values (see Fig. 29 right) shows a clear correlation for both unpolished and mechanically polished diamond coatings. A decreasing Vmp value leads to a decreasing wear rate. Vmp values lower than 0.04 ml/m² are associated with neglectable wear rates. The investigated impact of peak material volume of polycrystalline CVD-diamond coatings on dry friction against aluminum will be published in [26].

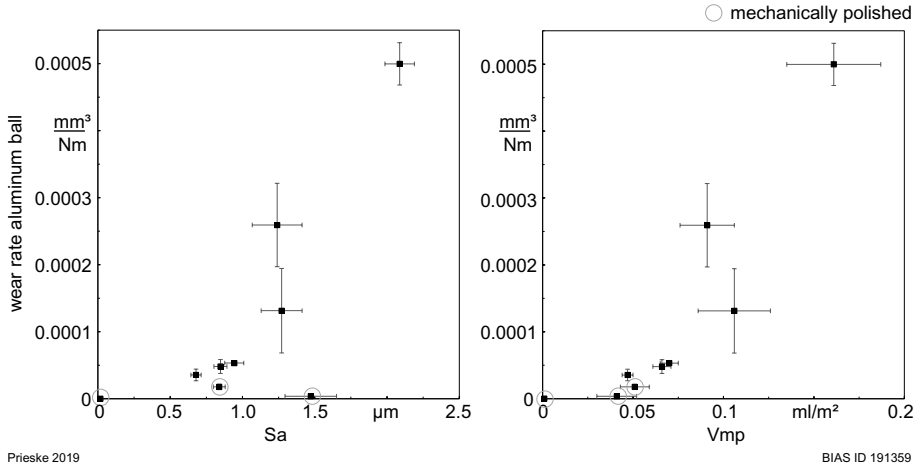

Fig. 29: Wear rate of the aluminum ball as a function of the arithmetical mean height as well as of the peak material volume.

In order to determine the forming degree of the tapering dies and the stamping velocity taper tests were carried out with uncoated hard metal (CTF12D) dies. In Fig. 30 the maximum forming force as function of the stamping velocity for lubricated and dry tapering of aluminum is shown. The tapering tests with uncoated tungsten carbide dies shows that a forming degree of 0.05 under lubricated conditions requires an average maximum forming force of 4 kN. With a forming degree of 0.08 the maximum forming force rises to about 5 kN. In addition, with a degree of forming of 0.05, the required maximum force is reduced by 0.7 kN as a result of an increase in the stamping velocity from 5 mm/s to 10 mm/s. In a dry forming process with a degree of deformation of 0.08, the process is already stopped during the first forming process at a force of 25 kN. With a degree of forming of 0.05, on the other hand, one workpiece can be produced with a maximum forming force of 6.6 kN. The second workpiece also reaches the abort criterion at 25 kN. Therefore, a die geometry with a degree of deformation of 0.05 was selected for the investigations with diamond coated taper dies.

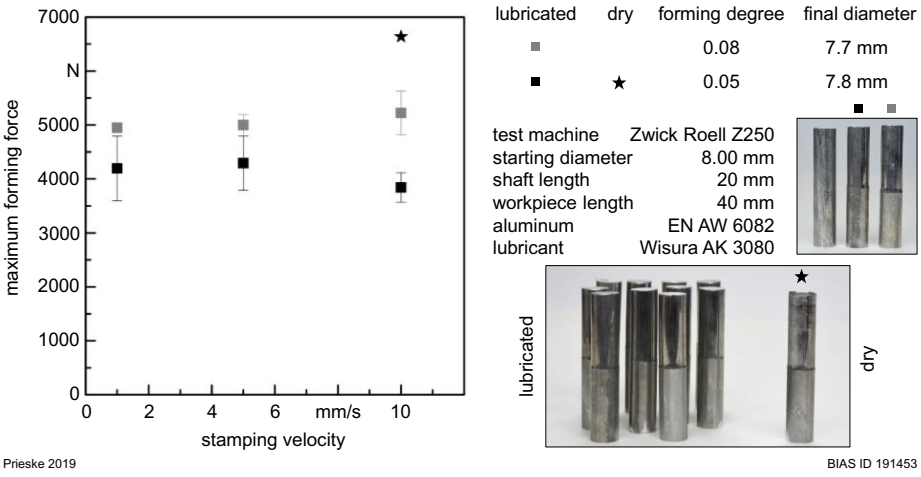

Fig. 30: Maximum forming force as function of the stamping velocity for lubricated and dry tapering of aluminum.

The result of laser polishing of a diamond coated forming die is shown in Fig. 31. Due to the exclusive accessibility from above the polishing process could only be carried out from one direction. In comparison to Fig. 22, the surface is therefore comparable to that after one polishing process (Fig. 22 middle). In addition, only the area of the die could be polished, which leads to a taper and allows a laser angle of incidence of 80°. The adjacent area of the die could not be polished due to a laser angle of incidence of 90°. Alternatively, the company ‘Diamond Product Solutions’ has tried to polish three dies mechanically using special tools. For all three dies, the mechanical polishing resulted in a delamination of the entire diamond coating.

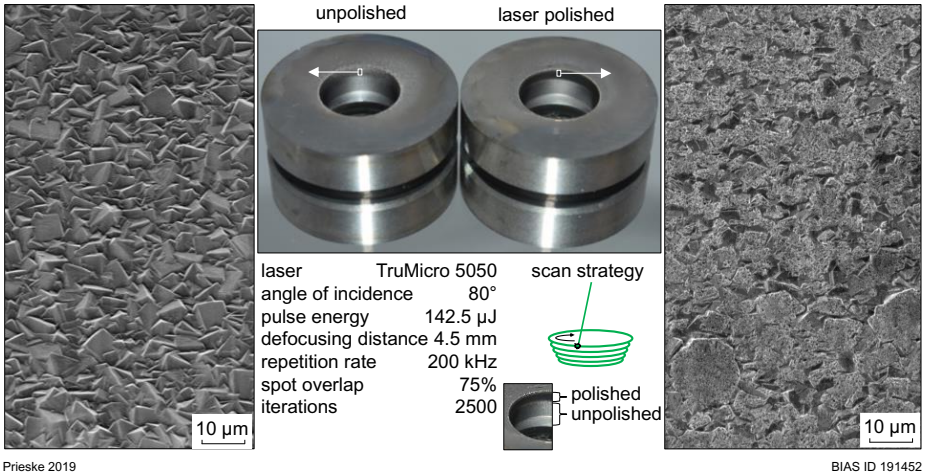

Fig. 31: Laser polishing of diamond coated forming die.

All tapering processes carried out with CVD diamond coated forming dies were stopped on the first workpiece at a forming force of 25 kN. To compare the different deposited CVD diamond coatings the shaft length of the workpiece after the forming process as function of the diamond quality factor is shown in Fig. 32. Due to the difficult accessibility of the diamond coating at the forming zone by a laser scanning microscope, no roughness measurements could be made, so that the diamond quality factor is used. The crystal sizes of the different CVD diamond coatings are all in the range of 1.88 µm ± 0.36 µm. The shaft length of the workpiece increases with a decreasing diamond quality factor and thus an increasing graphite content. The use of water or Wisura AK 3080 as lubricant with a CVD diamond coated forming tool with a diamond quality factor of 0.96 leads to an increase of the shaft length of at least 0.6 mm. The three laser-polished CVD diamond coated forming tools are polished with 400, 1000 and 2500 iterations. A polishing with 400 iterations leads to a shaft length of 3.45 mm. A further polishing with 1000 respectively 2500 leads to an improvement of the shaft length of about 1 mm. The analyses of the aluminum workpiece after the dry tapering test with a CVD diamond coated forming tool is shown in Fig. 33. First, it can be seen in Fig. 33 (top, middle), that a shaft length of 4.7 mm was successfully tapered. In addition, a bulge has formed and the initial diameter of the rod of 8.0 mm is thickened to 8.2 mm. After ejection of the workpiece the CVD diamond coating partly delaminated and sticks at the aluminum workpiece Fig. 33 (top, left). In the area of the tapering zone of the workpiece a clear imprint of the CVD diamond coating can be seen in Fig. 33 (bottom, left). Fig. 33 (right) shows an SE image of the aluminum workpiece where it exits the straight zone of the forming die. At the top part the imprint of the diamond coating can be seen which is followed by grooves.

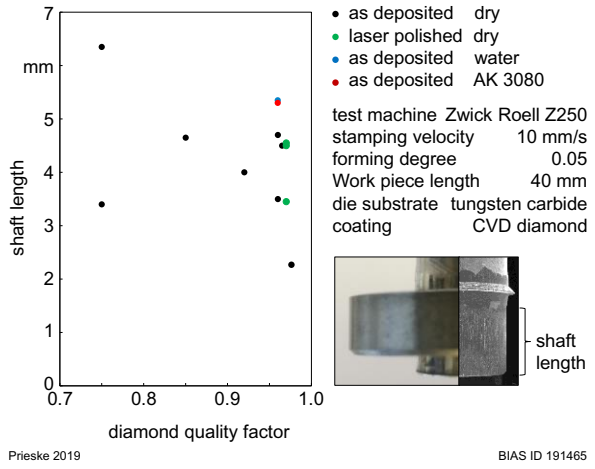

Fig. 32: Shaft length of the workpiece after tapering processes with CVD diamond coated forming dies as function of the diamond quality factor.

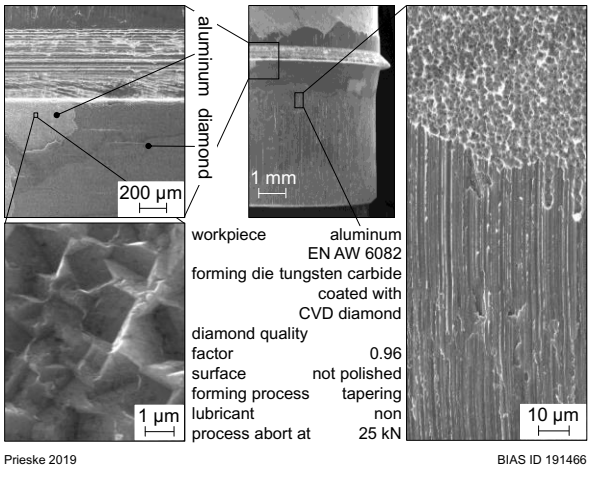

Fig. 33: Secondary electron images of the workpiece after the aborted tapering processes with a CVD diamond coated forming die.

4 Discussion

Looking at the process window (see Fig. 6), it is shown that no deposition takes place for low methane concentrations of 0.125%. In case of such low concentrations, the etching effect of the used hydrogen is high compared to the carbon deposition rate. The deposition of diamond coatings starts when increasing the methane concentration; hence, the diamond deposition rate lies above the etching rate. Thereby, the crystal size firstly also increases. For this region of the process window, Raman spectra of the samples show a clear Raman diamond line and only a comparatively small G-band graphite peak. This shows that most of the amorphous bound carbon, which is deposited besides diamond as well, is etched directly after its deposition by hydrogen. However, with further increasing methane concentrations, the crystal size again reduces. This decline of the crystal size is also described for hot-filament CVD processes on WC-Co substrates [27]. At this point, the etching rate of hydrogen is not high enough anymore to completely etch the partly deposited amorphous bound carbon. This could be seen in the Raman spectra of these samples, where the Raman diamond peak is reduced in intensity while the G-band graphite peak is more pronounced. The higher methane and graphite concentrations then lead to an increased number of secondary nucleation, and hence, to smaller crystal sizes. This higher number of smaller crystals, due to secondary nucleation at high methane concentrations, is also reported for thermal plasma CVD processes [28]. For low temperatures, the recombination processes of the process gases, before reaching the sample, lead to a smaller range of methane concentrations in which the above-described behavior takes place. For higher temperatures, higher methane concentrations could be used to deposit diamond coatings with low graphite content. This demonstrates that the recombination of unbound hydrogen is also reduced, and therefore, the etching rate increases for increasing temperatures. The etching effect is stronger for graphite since the bindings in graphite are less energetic than in diamond. For the processing time of 20 min and the temperature of 1050 °C, the maximum crystal size of 5.5 µm is reached at the methane concentration of 2.0%. With a diamond quality factor of 85%, compared to a quality factor of 100% for a pure diamond, still, a high concentration of sp^3-bonds is present at these processing parameters. The clear surface of the crystals in such coatings correlates with these findings. In comparison, microwave plasma CVD diamond coatings attain quality factors between 52% and 90%, depending on the process parameters [15]. Until a concentration of 3.0% is reached, the crystal size only decreases slightly to approx. 5.3 µm. For further increasing methane concentrations, the crystal size decreases to less than 1 µm for 5.0% methane. Hereby, the effect of a higher graphite content as well as the higher methane concentration, which leads to the formation of new crystal nuclei, can be observed. On the surface of such samples, amorphous phases are already visible. This is also noticeable in the diamond quality factor, which goes down to 62% for such coatings, hence showing a higher concentration of sp^2-bonds. In comparison to these results, [29] describes high graphite contents when depositing ultra-nanocrystalline diamond films in a hot-filament CVD process on silicon substrates. In conclusion, the working hypothesis that a wider range of methane concentrations can be used to deposit microcrystalline diamond coatings due to the increasing etching and deposition rate with rising deposition temperatures can be verified.

For increasing methane concentrations and increasing process temperatures, the coating thicknesses after the deposition for 20 min also increase. This correlation is also reported for hot-filament CVD processes [27]. The increase of the coating thickness can be explained similarly to the crystal sizes. For higher methane concentrations, the deposition rate of carbon increases compared to the etching rate of hydrogen. Therefore, higher coating thicknesses are reached at higher methane concentrations. This behavior, however, saturates in case of high methane concentrations. This is caused by the increasing graphite content of these coatings, which could be etched more effectively by the used hydrogen compared to the diamond. The described saturation is also reported in [30] for hot-filament CVD processes with silicon substrates, whereby higher graphite contents for higher methane concentrations are described. For increasing process temperatures, less recombination of the process gases takes place before reaching the substrate, and therefore more unbound carbon is present to form a coating. The same behavior is reported in [27,28] for hot-filament CVD processes, where it is described that higher deposition rates result at higher process temperatures due to the lower recombination of the process gases. For microwave plasma-enhanced CVD processes, additionally lower deposition rates for smaller temperatures are described [33]. For the process temperature of 1050 °C, the thickest coatings were observed. Interestingly, the thicknesses are significantly higher than those achieved at a process temperature of 1100 °C.

EDX-mappings on cryofractures of samples coated at 1100 °C show the beginning of the diffusion of the cobalt binder towards the surface of the substrate (Fig. 10). While the cobalt binder was etched 9 µm deep out of the surface to avoid a catalyzing effect during the coating process, it can now absorb more atomic carbon again, and thus, lead to delayed diamond nucleation at such high temperatures. These results correspond to the

findings reported in [34], which also describe a hindered diamond deposition by cobalt. Hereby, the catalytic effect of cobalt on the diamond growth and its respective transformation into graphite as well as the dissolvability of carbon in cobalt are of importance [35]. In addition, Haubner et al. [36] published that carbon starts to diffuse in hard metal at 800 °C and the amounts of tungsten and carbon, which are dissolved in the cobalt binder, increase with rising temperature. As a result, the solubility decreases strongly at approximately 1000 °C [36]. The diffusion of cobalt towards the surface of the substrate combined with the diffusion of carbon into the substrate and the dissolvability of carbon in cobalt lead to the strongly noticeable reduction of the deposited layer thicknesses when a process temperature of 1100 °C is reached. Due to this behavior, the process temperature of 1050 °C leads to the highest coating thicknesses after 20 min.

For the verification whether the coating thickness after 20 min can be transferred directly into a growth rate, depositions with the same process parameters and different deposition times were performed. The results show that the coating thicknesses behave linearly in correlation to the deposition time (see Fig. 11). The intersection point of the linear regression must pass through the zero point, since nucleation only begins when the coating process is switched on. In the first few minutes of the coating process it is possible that there is no linear growth due to diffusion processes. However, as soon as a closed CVD diamond layer is present and the diffusion processes of carbon from the plasma flame into the hard metal substrate are prevented, an almost linear growth follows due to the CVD process on the coating surface. For the conditions applied in experiments for Fig. 11, a growth rate of 0.36 µm/h is observed.

That knowledge enables the CVD diamond deposition with a desired coating thickness, whereby the deposition temperature and the crystal sizes can be chosen. In case of the CVD diamond deposition of a forming die it can be seen in Fig. 13, that a closed CVD diamond coating on the top flat area of the forming die leads to a delamination of the CVD diamond coating, which also leads to a spallation and crack formation at the inner wall of the forming die. Xu et al. [37] deposited CVD diamond coatings on cemented carbide substrates with smooth (Rq 0.04 µm) as well as blasted (Rq 0.27 µm) surfaces using a Cr-CrN interlayer system. In Rockwell C indentation tests the diamond coating without surface pre-treatment showed significantly poorer attachment (delamination at the interface to the interlayer); it was suggested that increased surface roughness prior to CVD diamond coating enhances layer adhesion [37]. In this study, this leads to the conclusion that the low roughness at the top area of the forming die is the cause of the delamination. The problem can be solved by masking that area during diamond nucleation, which results in a not closed diamond coating. In this way, no residual stresses can build up and in turn no flaking off occurs.

Fig. 15 shows that the growth rate decreases with increasing distance between the position to be coated and the plasma source. According to Corat et al. [31], the distance between substrate and plasma source at a fixed substrate temperature has a significant influence on the deposition rate, since at a greater distance the CH_3 molecules produced are already partially converted back to CH_4 molecules. At the distance of 7 mm, they detected a relative CH_3 concentration three times higher than at the distance of 11 mm. To overcome that problem in this study, the forming die was turned upside down in the middle of the deposition process, which resulted in the homogenous coating thickness of 2.3 µm ± 0.1 µm and the crystal diameter of 1.9 µm ± 0.2 µm.

To enable the postprocessing of the CVD diamond coatings the laser ablation of CVD diamond by a picosecond-laser was investigated and proved that polishing is possible, which was expected due to the feasibility of polishing by a femtosecond- [8] and nanosecond-laser [38]. The Raman spectra enables the comparison of the graphite content by the calculation of the ratio of I(diamond)/I(G). It could be shown that the ratio for the initial CVD diamond coating was the same as after one and four polishing processes, which means that no graphitization by the laser ablation by a picosecond-laser with a pulse duration shorter than 10 ps takes place.

The aim of the oscillating ball-on-plate tribometer tests is to find out whether a surface post-treatment of CVD diamond coatings is necessary for low-wear and low-friction in dry tribological contact with aluminum, the alloy EN AW-5083, or whether a targeted adjustment of the process parameters and the associated crystal size and surface roughness is sufficient. The hypothesis to be clarified is: For mechanically polished and non-polished polycrystalline diamond surfaces, a decrease in the wear rate of the aluminum counter body and the coefficient of friction due to a decrease in the topology size can be predicted with the help of a topology size, which takes into account the surface properties responsible for the mechanical interlocking and the abrasive wear. Several publications [4, 6] postulate that the lower the surface roughness of the CVD diamond layer, the lower the coefficient of friction and wear rate. Other publications [7, 39] doubt the direct relationship because the relationship is not present in the comparison between polished and untreated CVD diamond coatings. Hayward et al. [39] questions the measurement method of line roughness. On the one hand, different measuring

tips are used in different publications, which leads to different results for the same surfaces. In this work, instead of line roughness, surface roughness was measured with a laser scanning confocal microscope, which enables the evaluation of many other surface roughness parameters. The surface of the untreated CVD diamond layers differs mainly in the different crystal sizes. This leads to a scaling of most surface roughness parameters. The mechanically polished CVDD 10.25p coating achieves low values for all parameters due to the mirror-polished surface, so that in the diagrams it fits into the course of a decreasing coefficient of friction due to decreasing surface roughness parameters in Fig. 27. The rubbed CVD diamond coatings lead to inhomogeneous roughness parameters. The deep valleys of the microcrystalline CVD diamond layer are still present, but the protruding peaks have been greatly reduced, resulting in plateaus. The difference becomes particularly clear in Fig. 28 when comparing the CVDD 9.70 and the CVDD 8.89r coating. Rubbing two CVD diamond coatings with a mean diamond crystal size of 8.89 µm against each other reduces the mean arithmetic height Sa from 2.09 µm to 1.47 µm (by 30%), which is still the second highest value compared to the other coatings (Fig. 28 left diagram, the two values with the highest Sa). The peak material volume, however, was reduced from 0.161 ml/m² to 0.041 ml/m² (by 75%) and thus from the second highest to the second lowest value (see Fig. 28, right). In the diagram of the coefficient of friction as a function of the Vmp, the correlation can be seen that an increase in the Vmp leads to a near-to-linear increase in the coefficient of friction. From a Vmp value of about 0.1 ml/m², the coefficient of friction becomes saturated at about 0.5. Furthermore, the diagram shows that it is not to be expected that the coefficient of friction between the aluminum alloy EN AW-5083 and diamond will fall below 0.1.

From the diagram in Fig. 29 it can be concluded that the volume of the top 10% of the surface to which the peak material volume (Vmp) refers is the relevant factor for the abrasion of aluminum. Thus, the hypothesis could be confirmed. The topology size searched for, which for non-polished and mechanically polished CVD diamond coatings is equally capable of estimating the coefficient of friction as well as the wear rate of the aluminum counter body in the dry oscillating ball-on-plate tribometer test, is the peak material volume. For diamond coatings in dry contact with the aluminum alloy EN AW-5083, it can be concluded from the investigations that in order to minimize the wear rate of the aluminum counter body, a peak material volume of less than 0.04 ml/m² should be aimed for. The two untreated CVD diamond coatings with the lowest Vmp values (CVDD 0.48 and CVDD 0.94) exhibit layer delamination at the turning points. This means that they do not withstand repeated static friction. For this reason, the deposition of microcrystalline CVD diamond layers with subsequent post-treatment of the surface is recommended in order to achieve a peak material volume of less than 0.04 ml/m² for dry piece goods processes of aluminum workpieces.

By dry tapering of aluminum workpieces with CVD diamond coated forming dies a maximum shaft length of 6.3 mm was achieved with a diamond coating with a quality factor of 0.75. Fig. 33 clearly shows, that the adhesive wear by mechanical interlocking leads to a strong bond between the diamond coating and the workpiece. As a result, the aluminum workpiece is bulged and compressed. In addition, the diamond coating is partially detached during ejection. The ball on plate tribometer tests show, that a low Vmp value by polishing of microcrystalline CVD diamond coating in the whole contact zone would be promising. The accessibility by laser irradiation of the whole contact zone was not given. However, the polishing of the tapering zone alone already resulted in the shaft length of the workpiece being extended by 1 mm. By mechanical polishing of the CVD diamond coating the coatings delaminated, which means that the polishing process or the adhesion strength of the diamond coating needs to be improved to realize dry tapering of aluminum.

5 Conclusion

For the diamond deposition on K10 hard metal substrates (94% tungsten carbide, 6% cobalt), three conclusions can be drawn regarding the interaction of the deposition temperature and the methane concentration. It could be seen that wider ranges of methane concentration could be used to deposit microcrystalline CVD diamond coatings with increasing process temperature. The coating thickness saturates depending on the process temperature even though the methane concentration constantly increases. Furthermore, the coating thickness increases with increasing deposition temperature until the process temperature of 1100 °C at which the cobalt diffusion hinders the deposition. By turning a forming die upside down after half the coating time, so that the plasma flame enters through the other opening of the die, the entire inner wall of a 5 mm high forming die including undercuts was coated with a CVD diamond coating with homogeneous layer thickness and crystal diameter with a standard deviation of 0.1 µm and 0.2 µm, respectively. By laser polishing with a picosecond-laser the arithmetic mean height Sa of polycrystalline CVD diamond coatings could be reduced by 72.5% from 1.85 µm to 0.51 µm. It could be verified by Raman spectroscopy that the laser ablation process of CVD

diamond by a picosecond-laser with a pulse duration shorter than 10 ps can be performed without the formation of graphite. As soon as the CVD diamond coating is accessible by laser irradiation, the laser polishing process has a lower risk of delamination of the CVD diamond layer due to lower mechanical stress than applied by mechanical polishing.

For the overall vision of dry metal forming it could be shown, that the peak material volume (Vmp) is equally capable of estimating, for non-polished and mechanically polished CVD diamond coatings, the coefficient of friction as well as the wear rate of the aluminum counter body in the dry oscillating ball on plate tribometer test. For dry piece goods processes of aluminum workpieces, the deposition of microcrystalline CVD diamond layers with subsequent post-treatment of the surface is recommended in order to achieve a peak material volume of less than 0.04 ml/m² in order to minimize the wear rate of the aluminum counter body. The lower the Vmp value, the lower the coefficient of friction, so that a minimum Vmp value must be achieved in the case of a desired minimum coefficient of friction, which is limited for the dry contact of diamond with the aluminum alloy EN AW-5083 at 0.1.

Acknowledgements

The authors would like to thank the German Research Foundation (DFG Deutsche Forschungsgemeinschaft) for funding this work under the project number 390771352.

References

[1] F. Vollertsen, F. Schmidt: Dry Metal Forming: Definition, Chances and Challenges. Int. J. Precision Engineering and Manufacturing – Green Technology 1/1 (2014) 59-62.
[2] A.K. Chattopadhyay, P. Roy, A. Ghosh, S.K. Sarangi: Wettability and machinability study of pure aluminium towards uncoated and coated carbide cutting tool inserts. Surf. Coat. Technol. 203 (2009) 941–951
[3] 3 Better Ultra-hard materials Co., retrieved 30th September 2019 https://www.3betterdiamond.com/natural-diamond-dies
[4] B. Bhushan, V.V. Subramaniam, A. Malshe, B.K. Gupta, and J. Ruan: Tribological properties of polished diamond films. Journal of Applied Physics 74, 6, 4174 (1993)
[5] A. Erdemir, G.R. Fenske, C. Bindal, C. Zuiker, A.R. Krauss and D.M. Gruen: Friction and wear properties of smooth diamond films grown in fullerene-argon plasmas. In: 6th European Conference on Diamond, Diamondlike and Related materials, 1 (1995)
[6] A. Erdemir: Friction and wear of diamond and diamond-like carbon films. Proceedings of the Institution of Mechanical Engineers Part J: J Engineering Tribology 216, 387 (2002)
[7] U. Bögli, A. Blatter, S.M. Pimenov, E.D. Obraztsova, A.A. Smolin, M. Maillat, A. Leijala, J. Burger, H.E. Hintermann and E.N. Loubnin: Tribological properties of smooth polycrystalline diamond films. Diamond and Related Materials 4, 1009 (1995)
[8] T. Okuchi, H. Ohfuji, S. Odake, H. Kagi, S. Nagatomo, M. Sugata, H. Sumiya: Micromachining and surface processing of the super-hard nano-polycrystalline diamond by three types of pulsed lasers. Applied Physics A 96 (2009) 833-842
[9] M. Prieske, F. Vollertsen: In situ incorporation of silicon into a CVD diamond layer deposited under atmospheric conditions. Diamond and Related Materials 65 (2016) 47–52
[10] M. Prieske, C. Wiegmann, M. Schwander, F. Vollertsen: Feedback control of the substrate surface temperature in a laser-induced plasma CVD process. Dry Met. Form. OAJ FMT 1 (2015) 1–4
[11] M.G. Peters, R.H. Cummings: Methods for coating adherent diamond films on cemented tungsten carbide substrates. Patent US5236740A, 17 August 1993. Available online: https://patents.google.com/patent/US5236740A/en (accessed on 07 November 2019)
[12] V. Tokarev, J. Wilson, M. Jubber, P. John, D. Milne: Modelling of self-limiting laser ablation of rough surfaces: application to the polishing of diamond films. Diamond and Related Materials 4 (1995) 169–176
[13] A.C. Ferrari, J. Robertson: Raman spectroscopy of amorphous, nanostructured, diamond-like carbon, and nanodiamond. Math. Physi. Eng. Sci. 362 (2004) 2477–2512
[14] A.C. Ferrari, J. Robertson: Resonant Raman spectroscopy of disordered, amorphous, and diamond-like carbon. Phys. Rev. B 64 (2001) 1–13
[15] K.S. Pal, A.K. Mallik, N. Dandapat, N.R. Ray, S. Datta, S. Bysakh, B.K. Guha: Microscopic properties of MPCVD diamond coatings studied by micro-Raman and micro-photoluminescence spectroscopy. Bull. Mater. Sci. 38 (2015) 537–549
[16] M.P. Pereira, W.Y. Yan and B.F. Rolfe: Modeling of contact pressure in sheet metal forming. Materials Science Forum 561-565, 1975 (2007)
[17] Aluminium - Magnesium 5083. http://www.sabater-fundimol.com/customers/resources/pdf/sabater-fundimol_catalog_p28-29.pdf, Accessed: 25 October 2018
[18] M. Prieske, H. Hasselbruch, A. Mehner, F. Vollertsen: Friction and wear performance of different carbon coatings for use in dry aluminium forming processes. Surface & Coatings Technology 357 (2019) 1048-1059
[19] Lange, K.; Kammerer, M.; Pöhlandt, K.; Schöck, J.: Fließpressen – Wirtschaftliche Fertigung metallischer Präzisionswerkstücke. Springer Verlag Berlin Heidelberg, 1. Auflage (2008)
[20] C. Ramaswamy: The Raman effect in diamond. Nature 125, 3158 (1930) 704
[21] M. Prieske, S. Müller, P. Woizeschke: Interaction of methane concentration and deposition temperature in atmospheric laser-based CVD diamond deposition on hard metal. Coatings 9, 537 (2019) 1-10
[22] M. Prieske, F. Vollertsen: CVD diamond coating of forming dies with a homogenous coating thickness. Dry Met. Forming OAJ FMT 5 (2019) 9-12
[23] L. Bergman, R. J. Nemanich: Raman and photoluminescence analysis of stress state and impurity distribution in diamond thin films. Journal of Applied Physics 78, 11 (1995) 6709–6719
[24] J. Filik: Raman spectroscopy: a simple, non-destructive way to characterise diamond and diamond-like materials. Spectroscopy Europe 17, 5 (2005) 10-17
[25] M. Prieske, F. Vollertsen: Picosecond-laser polishing of CVD-diamond coatings without graphite formation. Special Issue Materials Today: Proceedings
[26] M. Prieske, A. Bohlen, F. Vollertsen: Impact of peak material volume of polycrystalline CVD-diamond coatings on dry friction against aluminum. JOM (under review)
[27] X.C. Wang, Z.C. Lin, B. Shen, F.H. Sun: Effects of deposition parameters on HFCVD diamond films growth on inner hole surfaces of WC-Co substrates. Trans. Nonferr. Metal. Soc. Chin. 25 (2015) 791–802

[28] Z.P. Lu, J. Heberlein, E. Pfender: Process study of thermal plasma chemical vapor deposition of diamond, part I: Substrate material, temperature, and methane concentration. Plasm. Chem Plasm. Process 12 (1992) 35–53
[29] D.C. Barbosa, F.A. Almeida, R.F. Silva, N.G. Ferreira, V.J. Trava-Airoldi, E.J. Corat: Influence of substrate temperature on formation of ultrananocrystalline diamond films deposited by HFCVD argon rich gas mixture. Diamond and Related Materials 18 (2009) 1283–1288
[30] K.K. Hirakuri, T. Kobayashi, E. Nakamura, N. Mutsukura, G. Friedbacher, Y. Machi: Influence of the methane concentration on HF-CVD diamond under atmospheric pressure. Vacuum 63 (2001) 449–454
[31] E.J. Corat, D.G. Goodwin: Temperature dependence of species concentrations near the substrate during diamond chemical vapor deposition. Journal of Applied Physics 74, 3 (1993) 2021–2029
[32] H. Matsubara, T. Sakuma: Diamond deposition on cemented carbide by chemical vapour deposition using a tantalum filament. J. Mater. Sci. 25 (1990) 4472–4476
[33] Y. Liou, A. Inspektor, R. Weimer, R. Messier: Low-temperature diamond deposition by microwave plasma-enhanced chemical vapor deposition. Appl. Phys. Lett. 55 (1989) 631–633
[34] R. Haubner, B. Lux: On the formation of diamond coatings on WC/Co hard metal tools. Int. J. Refract. Metal. Hard Mater. 14 (1996) 111–118
[35] R. Haubner, W. Kalss: Diamond deposition on hardmetal substrates—Comparison of substrate pre-treatments and industrial applications. Int. J. Refract. Metal. Hard Mater. 28 (2010) 475–483
[36] R. Haubner, W.D. Schubert, B. Lux: Interactions of hard metal substrates during diamond deposition. Int. J. Refract. Metal. Hard Mater. 16 (1998) 177–185
[37] Z. Xu, L. Lev, M. Lukitsch, A. Kumar: Effects of surface pretreatments on the deposition of adherent diamond coatings on cemented tungsten carbide substrates. Diamond and Related Materials 16, 3 (2007) 461–466
[38] S. M. Pimenov, V. V. Kononenko, V. G. Ralchenko, V. I. Konov, S. Gloor, W. Lüthy, H. P. Weber, A. V. Khomich: Laser polishing of diamond plates. Applied Physics A: Materials Science & Processing 69 (1999) 1, 81–88
[39] I.P. Hayward: Friction and wear properties of diamonds and diamond coatings. Surface and Coatings Technology 49, 554 (1991)